JOURNAL OF SPACECRAFT AND ROCKETS
Vol. 43, No. 3, May–June 2006

Steering Moments Creation in Supersonic Flow by Off-Axis Plasma Heat Addition

I. G. Girgis,* M. N. Shneider,† S. O. Macheret,‡ G. L. Brown,§ and R. B. Miles¶
Princeton University, Princeton, New Jersey 08544

The change in aerodynamic forces as a result of local plasma heat addition to supersonic flow (Mach 3.0), upstream of a cone, is studied numerically by solving the three-dimensional compressible Euler equations. In principle, such an effect on the forces and moments can be used for vehicle steering as well as drag reduction. Local energy addition to the flow is achieved by the use of microwave radiation as a heating-source and an electron beam to control the air conductivity and consequently the location of the energy deposition. This approach requires heating only in a localized preionized region, and so the strength of the microwave field has to be much lower than the critical value of the electric field at breakdown. Results show the potential effects of heat addition on the aerodynamic forces. The corresponding power and the optimized location required to achieve these effects are discussed.

Nomenclature

A = cone cross-sectional area
C = constant, 4×10^{-21} (keV · m)^2
CD = drag coefficient
CD_0 = drag coefficient in absence of heat addition
CL = lift coefficient $= L_f/(0.5\rho_\infty u_\infty^2 S)$
D = cone diameter
E_a = electric field amplitude
$E_{a,c}$ = breakdown field strength
j_b = electron beam current densities
L = cone length
L_{ext} = extrapolated beam relaxation length
L_f = lift force
M_∞ = mach number
N = averaged path gas number density, m^{-3}, along the beam propagation
n_e = electron number density
P = power of heat disposition
P_D = total kinetic energy flux over an area A equal to the cross-sectional area of the body, $= 0.5\rho_\infty u_\infty^3 A$
p_∞ = freestream pressure
Q = dimensional power density
q = nondimensional power density
R = heat deposition location radius
r_{eff} = effective heating radius
r_s = plasma effective radius
r_0 = beam radius at the injection point (i.e., the radius of the window)
S = body projected area on the symmetry plane
u_∞ = freestream velocity
δ = skin layer thickness
ε_b = initial electron beam energy, keV
η = microwave energy fraction
θ = heat deposition location angle
μ_e = electron mobility
ξ = electron beam focusing parameter by an external magnetic field
ρ_∞ = freestream density
σ = plasma conductivity

Presented as Paper 2002-0129 at the AIAA 40th Aerospace Sciences Meeting, Reno, NV, 14–17 January 2002; received 18 March 2005; revision received 8 July 2005; accepted for publication 25 July 2005.

*Lecturer, Mechanical and Aerospace Engineering. Associate Fellow AIAA.
†Research Scientist, Mechanical and Aerospace Engineering. Senior Member AIAA.
‡Senior Research Scientist, Mechanical and Aerospace Engineering. Associate Fellow AIAA.
§Professor, Mechanical and Aerospace Engineering. Associate Fellow AIAA.
¶Professor, Mechanical and Aerospace Engineering. Fellow AIAA.

I. Introduction

HIGH-SPEED vehicles performance can be improved in different ways, for example, by transition delay and control, by shape optimization, and by heat addition. In this paper we explore the concept of using electron-beam-controlled microwave heat addition for drag reduction and for creation of steering moments. Because the heat added in this manner can be electronically controlled, it has several advantageous characteristics such as spatial accuracy, rapid response, and flexibility. This work was conducted to illuminate the concept and has provided guidance to ongoing aerodynamic control experiments in a Mach 3 tunnel at Princeton.[1–4] No attempts were made to study system integration issues.

Over the years, a number of studies have been devoted to the effects of heat addition on supersonic and hypersonic flows.[5–15] Among most recent studies are those of sonic boom suppression,[16] electron-beam energy addition and magnetohydrodynamic (MHD) power generation and extraction,[17] high-speed flow control by microwave driven plasma discharges,[1–4] and active MHD shock control in a scramjet inlet.[18] Furthermore, drag reduction by a plasma air spike in front of a vehicle has recently received attention.[19,20]

In this study, the change in aerodynamic forces as a result of local heat addition to supersonic flow is studied numerically. The electron-beam-controlled microwave energy is deposited in front of the vehicle to create steering moments as well as to reduce drag. This concept might eventually reduce the number or size of control surfaces of a high-speed vehicle and would offer flexibility for vehicle control.

The following sections outline descriptions of the body configuration, numerical methods, and steps that have been taken to determine the optimum location for maximum drag reduction and steering moment, for a given energy deposition power.

II. Problem Description and Numerical Simulation

In the present work, a three-dimensional compressible Euler solver, originally developed by Martinelli et al.,[21] is used, where the heating term is incorporated in the energy equation. The flow is computed over a 15-deg half-angle cone. The cone configuration is shown in Fig. 1. A C-H mesh is constructed over half of the cone using a mesh of $129 \times 49 \times 49$ grid points in x, y, z (Fig. 2). The

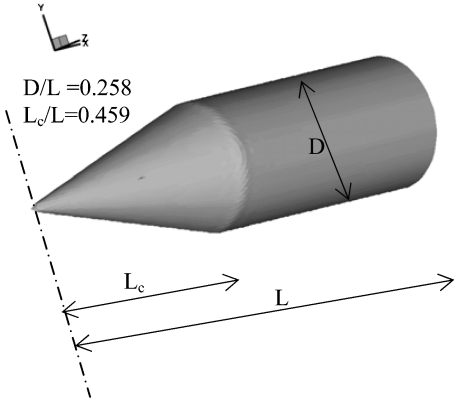

Fig. 1 Cone configuration.

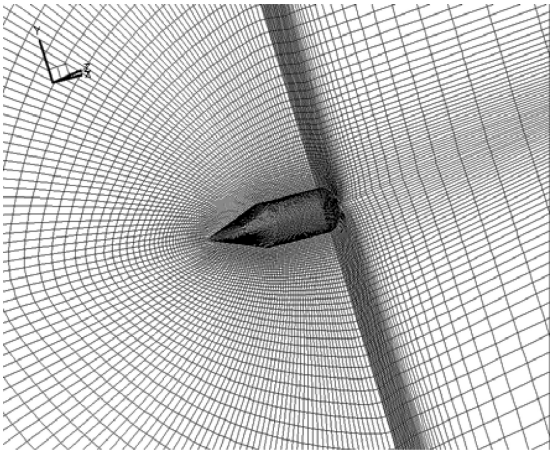

Fig. 2 Mesh arrangement.

distance from the body to the outer boundary is three chord lengths on each side. The tip of the cone was slightly altered to obtain an orthogonal mesh. Because the base drag is dependent on the tail geometry and should not be significant for powered high-speed flights, its effect was not included in this study.

The governing equations are discretized using a second-order, cell-vertex, finite volume scheme in space. Integration of the governing equations in time, using a four-stage Runge–Kutta scheme, is employed until a steady-state solution is reached. The Jameson–Schmidt–Turkel scheme[21] is used to effectively capture shock formation.

Major enhancement in the convergence rate to a steady-state solution is achieved using the multigrid, local time-stepping, technique.[22] Moreover, residual smoothing is used for further acceleration to the steady-state solution in which the high-frequency noise, generated by the multigrid transfer cycles, is damped out.

A grid-refinement study is conducted to ensure a grid-independent solution. Three mesh arrangements are used in this study. The coarse, medium, and fine mesh have $33 \times 13 \times 13$, $65 \times 25 \times 25$, $129 \times 49 \times 49$ grid points in x, y, z, respectively. It is found that the code converges to a unique solution as we increase the mesh points, and the error in the drag coefficient is less than 1% between the medium and the fine mesh.

III. Model of Spatial Profiles of Electron-Beam and Microwave-Induced Heating

Fully self-consistent three-dimensional computations of electron-beam propagation and scattering, beam-induced ionization, redistribution of the microwave field caused by the plasma generation, and absorption of microwave power, accompanied by gas heating and vibrational excitation, would be extremely difficult if at all possible. In this work, several simplifying assumptions have been adopted.

The electron number density in the plasma produced by the e-beam is $n_e \sim 10^{10}$–10^{11} cm^{-3} at typical available beam current densities, $j_b < 1$ mA/cm^2. For those n_e values, a typical microwave source electric field frequency of 2.45 GHz, and a skin layer thickness δ of the order of the plasma region scale (which is the case for small-scale experiments ~1–5 cm), we consider gas heating by the microwave field in the entire plasma region created by the e-beam, with the volumetric heating rate:

$$Q_E = \eta\sigma E_a^2/2 = \eta e \mu_e n_e E_e^2/2 \tag{1}$$

where η is the fraction of microwave energy absorption that goes into heating (not to excitation, dissociation, etc.).

Furthermore, the low electron density allows us to neglect the distortion of the electric field in the plasma region and to consider E_a to be constant at a given location. Estimates show that heating by the microwave subcritical field $E < E_{a,c}$ is much more intense than that by the e-beam itself. However, the ionization rate and the conductivity are predominantly caused by high-energy beam electrons, not to the plasma electrons heated in the microwave field. Therefore, we shall neglect microwave internal ionization and assume that the microwave-heating region coincides with the ionized region produced by the e-beam.

With the preceding assumptions, the microwave heating rate, according to Eq. (1), is proportional to the electron density generated by the electron beam. In turn, the quasi-steady-state electron density is determined by the beam-induced ionization rate that is proportional to the beam power deposition rate and by the rate of electron losses.

The latter can be either linear (for convective electron removal) or quadratic (for the recombination loss mechanism) with respect to n_e. For centimeter-scale plasma regions, flow velocities of several hundred meters per second, and electron densities $n_e \le 10^{11}$cm^{-3}, convective electron removal is the prevailing loss mechanism, and the quasi-steady-state electron density is proportional to the beam power deposition rate.

Thus, the microwave heating rate will be assumed to be proportional to the beam power deposition rate in this paper. However, one has to bear in mind that for larger plasma regions and higher electron densities the recombination loss mechanism would become important, and the microwave heating rate would be proportional to the square root of the e-beam power deposition rate.

Shneider et al.[18] have demonstrated that electron-beam power deposition and the ionization rate can be described by a Gaussian profile along the beam propagation path when the beam propagation is parallel to a strong magnetic field. To allow for radial spreading of the beam as a result of angular scattering in elastic collisions, the microwave heating rate, proportional to the beam-induced ionization profile, is approximated in this work by the following Gaussian function of both longitudinal s (distance along the beam) and transverse r coordinates:

$$Q = A_c \exp\left[-2(s - s_0)^2/\chi^2\right] \exp\left[-\xi\left(r^2/r_s^2\right)\right] \text{W/m}^3 \tag{2}$$

where $s_0 = L_{\text{ext}}/3.21$ and $\chi = 0.65 s_0$ and $\xi \approx 1$–10^{15}. Specifically, $\xi = 1$ corresponds to the absence of beam focusing, and $\xi > 1$ in the case of focusing by an external B-field parallel to s. The values of s_0 and χ are chosen based on Monte Carlo calculations conducted by Shneider et al.[18] at the same present conditions. The constant A_c can be determined from the normalization condition:

$$P = \int_0^\infty \int_0^\infty 2\pi r\, Q(r, s)\, \mathrm{d}s\, \mathrm{d}r \tag{3}$$

The key parameters in the Gaussian profile, Eq. (2), can be related to the energy of the electron beam and the gas density. For a uniform-density gas, convenient empirical formulas for L_{ext} and r_s have been suggested by Bychkov et al.[23] The same approximations for the extrapolated length and the effective radius of e-beam scattering were assumed to be valid for a spatially nonuniform gas density:

$$L_{\text{ext}} = 1.1 \cdot \frac{10^{21}\varepsilon_b^{1.7}}{\bar{N}} \tag{4}$$

$$r_s^2 = \left(r_0^2 + \frac{C\bar{N}s^3}{\varepsilon_b^2}\right) \tag{5}$$

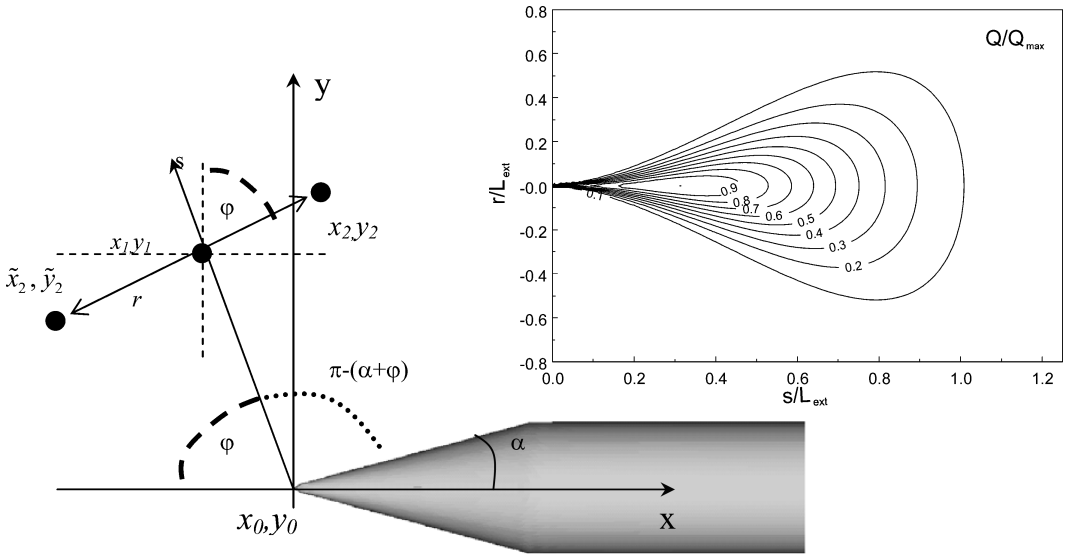

Fig. 3 Illustration of the coordinate transformation from the physical coordinate system (x, y) to the (s, r) coordinate system and the normalized power density (Q/Q_{max}) profile with $\zeta = 4$ at the symmetry plane.

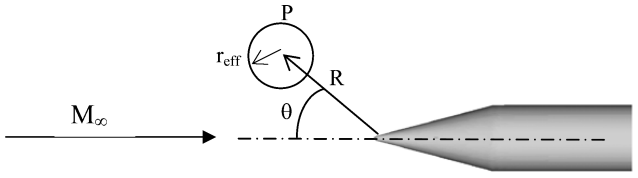

Fig. 4 Variables of the parametric study.

$$\bar{N} = \frac{1}{L_{\text{ext}}} \int_0^{L_{\text{ext}}} N(s)\, \mathrm{d}s \tag{6}$$

In Eqs. (4) and (5), s, r_0, L_{ext}, and r_s are in meters and ε_b is keV.

Equations (4) and (6) give the equation for L_{ext} at a given ε_b and a specified number density distribution $N(s)$:

$$\int_0^{L_{\text{ext}}} N(s)\, \mathrm{d}s = 1.1 \cdot 10^{21} \varepsilon_b^{1.7} \tag{7}$$

When coupling the calculations of the heating profile with computational fluid dynamics (CFD) modeling, the beam coordinates (s, r) have to be expressed in terms of the physical coordinates (x, y, z). Figure 3 illustrates a two-dimensional transformation, at the cone symmetry plane, where the electron beam is injected from the vertex of a cone, at an arbitrary angle φ with respect to the x axis. Denoting the vertex coordinates as (x_0, y_0), and (x_1, y_1) as an arbitrary point along s, for a point (x_2, y_2) in the symmetry plane, such that $x_2 \geq x_1$, $y_2 \geq y_1$, the transformation equation will be

$$s = -(x_2 - x_0)\cos\varphi + (y_2 - y_0)\sin\varphi, \qquad s \geq 0$$

$$r = (y_2 - y_0)\cos\varphi + (x_2 - x_0)\sin\varphi, \qquad r \geq 0 \tag{8a}$$

Similarly, for a point ($\tilde{x}_2$, $\tilde{y}_2$), such that $\tilde{x}_2 < x_1$, $\tilde{y}_2 < y_1$, the transformation equation will be

$$s = (x_0 - \tilde{x}_2)\cos\varphi + (\tilde{y}_2 - y_0)\sin\varphi, \qquad s \geq 0$$

$$r = -(\tilde{y}_2 - y_0)\cos\varphi + (x_0 - \tilde{x}_2)\sin\varphi, \qquad r \geq 0 \tag{8b}$$

These transformation equations were extended in the z direction to describe the three-dimensional heating profile in the (x, y, z) coordinates. In the present calculations, the ε_b was varied from 10 to 25 keV to create a beam relaxation length L_{ext}, comparable with the cylinder diameter D. The radius of the e-beam window was set to 10^{-3} m ($r_0 \ll D$), which is a realistic size for an e-beam aerodynamic window without a membrane.

IV. Discussion of the Results

Drag reduction and steering moments for a given vehicle geometry and flow conditions depend on many parameters. Location (R and θ), effective heating radius, and the power of the heat deposition were the variables investigated here, as shown in Fig. 4. In this study, only one body configuration is employed, a 15-deg half-angle cone with the center of heat addition on its symmetry plane ($z = 0$). In most of the study, a freestream Mach number of 3.0 was used with zero angle of attack.

A. Spherical Gaussian Heat Addition

To understand the heat addition effects, a parametric study was conducted to examine the effect of different parameters on the body's drag and lift. Before using an attainable electron-beam-controlled microwave heating profile, a spherical Gaussian heating profile was utilized. In this study, the heating power was normalized by the flux of kinetic energy in the freestream through a cross-sectional area equal to that of the body.

In the first series of computations, the spherical heat addition was located in front of the cone nose, on the x axis ($\theta = 0$), at different distances R to find the location that results in the maximum drag reduction for a given power. For such a case, the energy must be deposited far enough upstream of the cone to permit the air to be deflected ahead of the attached shock, but not too far upstream, or otherwise the effect will be reduced.

For $M_\infty = 3.0$, $P/P_D = 1.0$, and $r_{\text{eff}}/D = 0.2$, R/D was varied from approximately 0.04 to 1.75. As seen in Fig. 5, the maximum drag reduction, $CD/CD_0 = 0.65$, occurs at $R/D)_{\text{opt}} \sim 0.4$. With this on-axis heat addition, $CL/CD = 0.0$.

In the second series of computations, at fixed $R/D = R/D)_{\text{opt}}$, r_{eff}/D was varied from 0.15 to 0.4. As shown in Fig. 6, the effective heating radius has a significant effect on drag reduction. For this case as r_{eff}/D is reduced, the drag reduction initially increases because the flow is heated and deflected more ahead of the cone. The effect was diminished for $r_{\text{eff}}/D < 0.2$, and there is a small difference between 0.15 and 0.2: $CD/CD_0)_{\min} \sim 0.65$. Because of mesh restrictions, the smallest value of r_{eff}/D was limited to 0.15. For resolution and accuracy reasons, the $r_{\text{eff}}/D)_{\text{opt}} = 0.2$ was used.

The optimum case for drag reduction is shown in Fig. 7, where the contours of the nondimensional pressure distribution p/p_∞ are plotted in Fig. 7a. As expected, the heat addition region increases the temperature and decreases the Mach number ahead of the cone and acts to deflect the upcoming high-speed flow and ultimately turn the flow through weaker shocks.

Because the velocity components are nondimensionalized by $(p_\infty/\rho_\infty)^{0.5}$ and the length by L, the nondimensional power density is written as $q = Q/[p_\infty^{1.5}/(\rho_\infty^{0.5} L)]$ and is plotted in Fig. 7.

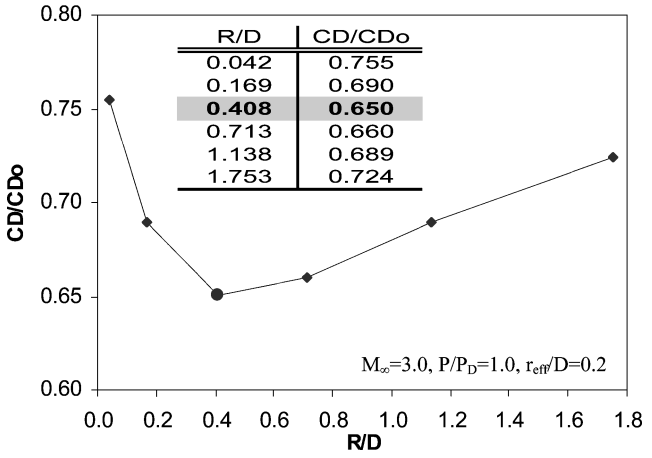

Fig. 5 Heating location effect on drag reduction.

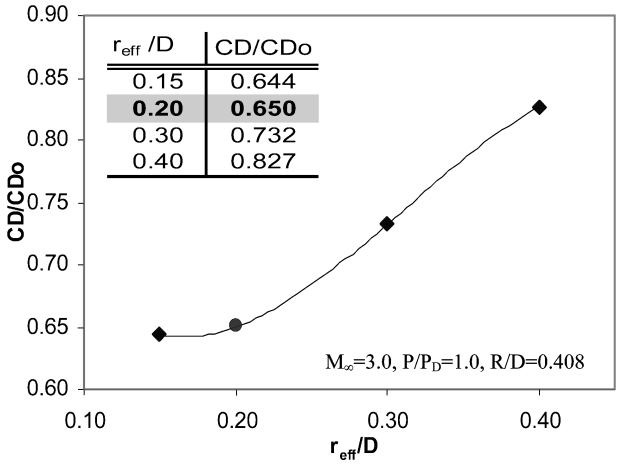

Fig. 6 Effective heating radius effect on drag reduction.

In the third series of computations, subsequent to determining the optimum effective heating radius and distance, heat was deposited off the cone axis to generate a steering moment. Therefore, the angle θ was changed from 0 to 75 deg, using $r_{\text{eff}}/D)_{\text{opt}} = 0.2$ and $R/D)_{\text{opt}} \sim 0.4$. The optimum angle $\theta)_{\text{opt}}$ corresponding to the maximum value of CL/CD, was found to be between 40 to 50 deg. This maximum value $(CL/CD)_{\max}$ is approximately 0.6, as shown in Fig. 8.

In that case, the shock wave associated with the heat addition interacts with a small region on the upper surface of the cone. To avoid hot spots and shock impingement to the tip of the cone, the heating source was moved slightly away from the cone ($R/D \sim 0.64$ and $\theta \sim 28$ deg (Fig. 9). In this case the obtained steering force, $CL/CD = 0.56$, is still close to that in the optimum case ($CL/CD = 0.59$). Figure 9 shows that the heat-generated shock wave merges with the lower shock wave of the cone and slightly strengthens it, while the heating weakens the upper shock wave of the cone, especially away from the nose of the cone.

All of the preceding calculations were conducted using a high rate of heat addition, $P/P_D = 1.0$. To explore the possibility of creating steering forces at various power levels, and whether it is more beneficial to add energy in front of the cone rather than in the propulsion system, different P/P_D values were used, as shown in Fig. 10. The highest gain in CL/CD is achieved, of course, with the highest power. However, CL/CD gain does not grow linearly with P/P_D.

Finally, to study the effect of Mach number on the steering force, Fig. 11 shows the substantial effect of Mach-number increase on the steering force. Because it takes numerous simulations to obtain the optimum heating location, the results at $M_\infty = 5.0$ are not as well optimized as of $M_\infty = 3$ and 2.4. It is clear that a considerable gain in steering moment can be achieved at high Mach numbers. Because the pressure jump across a shock wave is proportional to

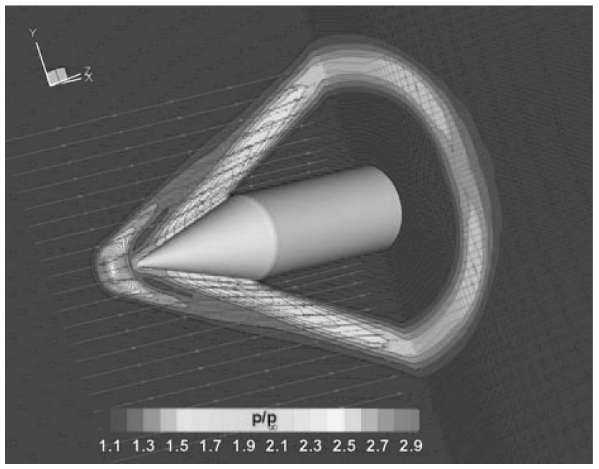

a)

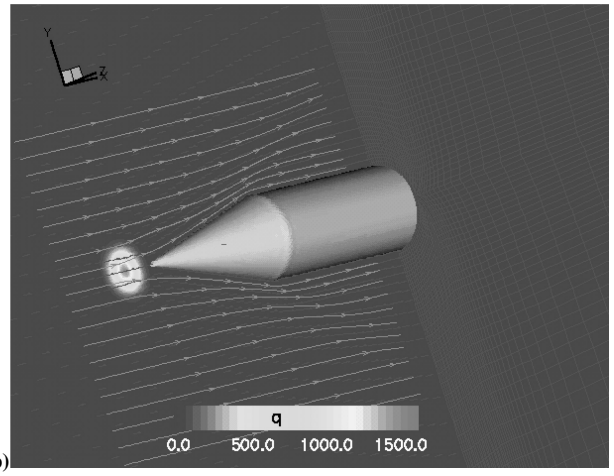

b)

Fig. 7 Optimum case for drag reduction ($M_x = 3.0$, $P/P_D = 1.0$, $R/D = 0.408$, $\theta = 0$ deg, $CD/CD_0 = 0.65$, and $CL/CD = 0.00$): a) pressure distribution and b) power density around the cone.

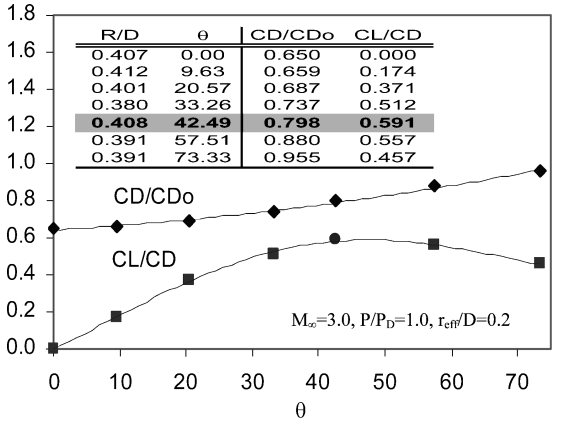

Fig. 8 Heating angle effect on steering force.

M_∞^2, at high Mach number, the drag reduction as a result of heating and a corresponding Mach number change ΔM, is approximately proportional to $2\, M_\infty \Delta M$, where, as discussed by McAndrew,[1] for a simple Rayleigh flow for fixed static pressure and volumetric heat addition ΔM is a weak function of Mach number. Figure 11 supports this approximation and shows that C_L/C_D increases approximately linearly with Mach number. Thus, heat addition at hypersonic speeds could be a possible solution for the improvement of vehicle performance.

B. Electron Beam and Microwave-Induced Heat Addition

In this section, the modeling of the spatial profile of the electron beam and the microwave-induced heating is considered. Based on

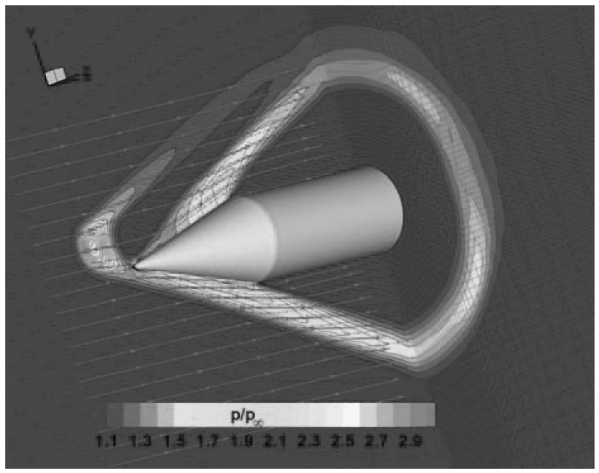

a)

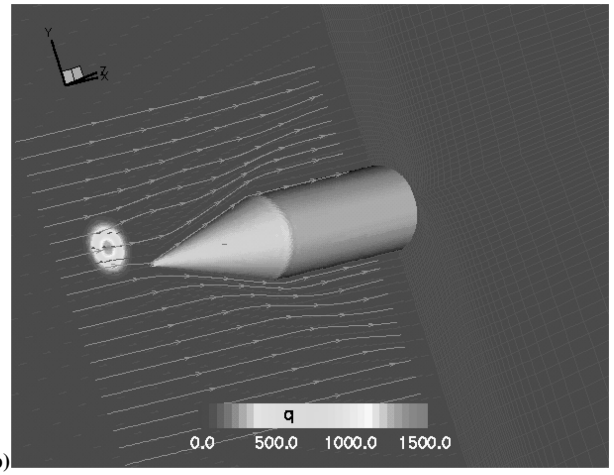

b)

Fig. 9 Optimum case for creation of steering force ($M_\infty = 3.0$, $P/P_D = 1.0$, $r_{eff}/D = 0.2$, $R/D = 0.64$, $\theta = 28$ deg, $CD/CD_0 = 0.76$, and $CL/CD = 0.56$): a) pressure distribution and b) power density around the cone.

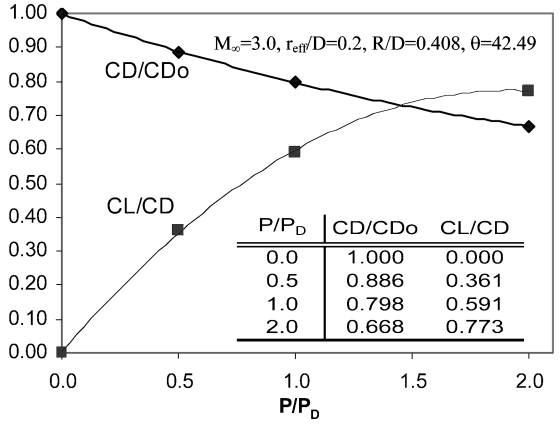

Fig. 10 Power effect on steering force.

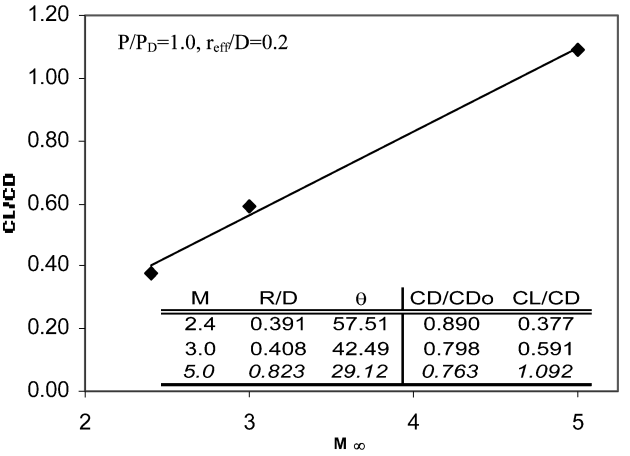

Fig. 11 Mach-number effect on steering force.

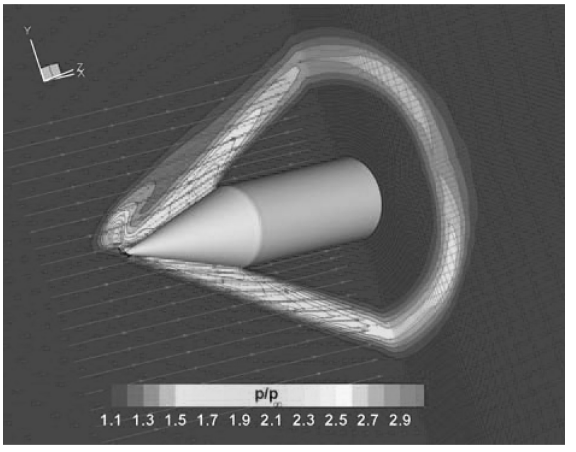

a)

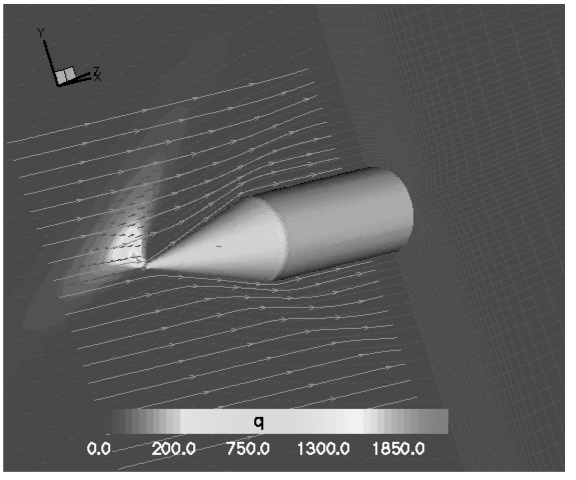

b)

Fig. 12 Optimum case for creation of steering force using electron-beam and microwave-induced heat addition ($M_\infty = 3.0$, $P/P_D = 1.0$, $L_{ext}/D = 0.2$, $\theta = 60$ deg, 20 keV, $CD/CD_0 = 0.88$, and $CL/CD = 0.42$): a) pressure distribution and b) power density around the cone.

the results obtained in the preceding section, the extrapolated beam relaxation length of $L_{ext}/D = 0.2$ and electron-beam focusing parameter of $\xi = 4$ for a 20-keV electron beam were used. The optimum electron beam angle is found to be approximately 60 deg. Because the electron-beam heating profile is not focused as much as the spherical Gaussian heating profile, the corresponding drag reduction and steering force gain ($CD/CD_0 = 0.88$ and $CL/CD = 0.42$), for this flow (Fig. 12) are not as large as the values obtained with the spherical Gaussian heating profile. The pressure distribution along the x axis and over the cone surface for this case is plotted in Fig. 13. As a result of the off-axis heat addition, a pressure drop occurs on the upper surface of the cone. In this case, the pressure p/p_∞ is reduced to as small as 1.6 compared with 2.0 in the absence of heat addition. The weakening of the upper surface shock wave is the main mechanism for creating the steering force on the cone. The peak in pressure at the cone tip is caused by the tip geometry, which has an angle that is slightly larger than the cone half-angle in order to satisfy orthogonal grid requirements.

A photograph of the plasma and the test section from the experimental work done by McAndrew et al.[3] is shown in Fig. 14. The flow is from left to right, and the cone can be seen on the right-hand

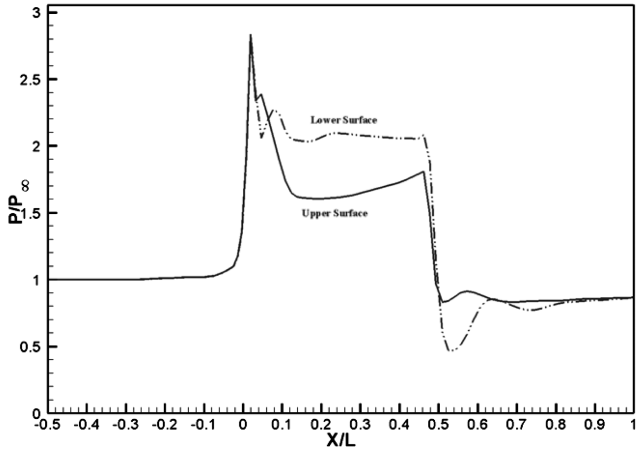

Fig. 13 Pressure distribution along the centerline and over the cone upper and lower surfaces, using electron-beam and microwave-induced heat addition, creation of steering force optimum case ($M_\infty = 3.0$, $P/PD = 1.0$, $L_{ext}/D = 0.2$, $\theta = 60$ deg, 20 keV, $CD/CD_0 = 0.88$, and $CL/CD = 0.42$).

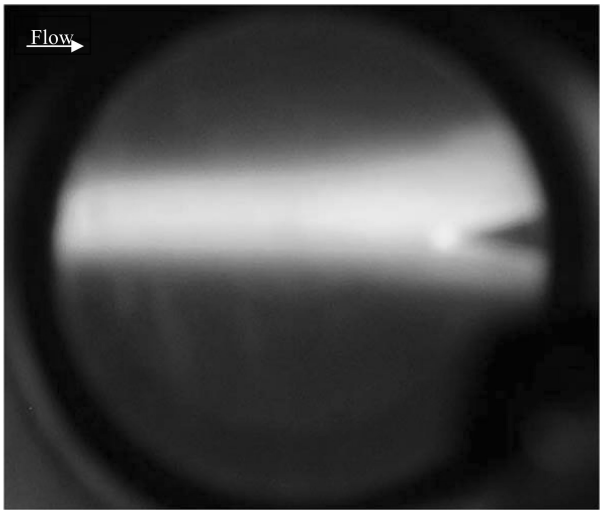

Fig. 14 Plasma over a 15-deg cone in Mach 3 flow.[1]

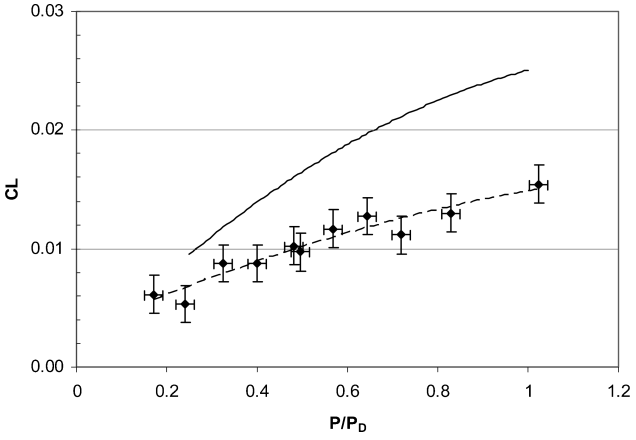

Fig. 15 Lift coefficient vs normalized power.[1]

side. The photograph shows the plasma flowing past the cone with a visible corona discharge at the tip of the cone. Figure 15 shows the results obtained by McAndrew[1] for the lift coefficient CL vs the normalized power P/P_D. These results compare reasonably with the current work. For example, at $P/P_D = 1.0$ the experimental lift coefficient is about 0.0154 ± 0.0016 compared with 0.025 from the present work. A larger lift coefficient for the CFD prediction is expected because in the calculations it is much easier to optimize both the heat addition profile and its location. Based on the chart provided by Sims,[24] the lift coefficients shown in Fig. 15 would correspond to angles of attack of approximately 1 to 3 deg.

V. Conclusions

A full, three-dimensional, inviscid numerical simulation has been performed to understand and determine the effect of adding heat ahead of a cone at Mach 3, on drag reduction and the creation of a steering force. A nondimensional parametric study was carried out to determine the optimum location of the heat addition as well as the effects of heat addition power and Mach number. Potential effects on the steering force and drag reduction are reported. Specifically, when using a heating power equivalent to $0.5\rho_\infty u_\infty^3 A$ and the volumetric heating parameters of this study, the drag can be decreased to only 88% of the drag in absence of the heat addition. Moreover, the lift coefficient can be increased to $\sim 0.42 CD$. These effects are enhanced as the Mach number increases. Experimental work demonstrated this concept in a small Mach 3 facility. Preliminary experimental results[1] show fair agreement with the current numerical results.

Acknowledgment

This work was supported by Research Support Instruments, Inc., under a Small Business Innovation Research grant from the U.S. Air Force Research Laboratory.

References

[1]McAndrew, B., "Aerodynamic Control in Compressible Flow Using Microwave Driven Discharges," Ph.D. Dissertation, Mechanical and Aerospace Engineering, Princeton Univ., Princeton, NJ, June 2003.

[2]McAndrew, B., Sullivan, D., Kline, J., Fox, J., and Miles, R. B., "Supersonic Flow Control by Microwave Driven Plasma Discharges," AIAA Paper 2002-0354, 2002.

[3]McAndrew, B., Kline, J. F., and Miles, R. B., "Aerodynamic Control of a Symmetric Cone in Compressible Flow," AIAA Paper 2003-33, 2003.

[4]McAndrew, B., Barker, P., and Miles, R. B., "Development of a Supersonic Plasma Wind Tunnel," AIAA Paper 2000-0533, 2000.

[5]Bushnell, D. M., "Supersonic Aircraft Drag Reduction," AIAA Paper 90-1596, 1990.

[6]Batdorf, S. B., "On Alleviation of the Sonic Boom by Thermal Means," AIAA Paper 70-1323, 1970.

[7]Miller, D. S., and Carlson, H. W., "On the Application of Heat or Force Field to the Sonic-Boom-Minimization Problem," AIAA Paper 70-903, 1970.

[8]Marconi, F., "An Investigation of Tailored Upstream Heating for Sonic Boom and Drag Reduction," AIAA Paper 98-0333, 1998.

[9]Levin, V., and Terenteva, L., "Supersonic Flow over a Cone with Heat Release in the Neighborhood of the Apex," *Izvestia Rossiiskoi Akademii Nauk–Mekhanika Zhidkosti i Gaza*, No. 2, March–April 1993, pp. 110–114 (in Russian).

[10]Georgievsky, P. Y., and Levin, V. A., "Supersonic Flow over a Body with a Heat Supply Ahead of It," *Proceedings of the Steklov Institute of Mathematics*, No. 1, American Mathematical Society, 1991, pp. 229–234.

[11]Vlasov, V. V., Grudnitskii, B. G., and Rygalin, V. N., "Gas Dynamics with Local Energy Release in Subsonic and Supersonic Flow," *Fluid Dynamics*, Vol. 30, No. 2, 1995, pp. 275–280.

[12]Riggins, D., Nelson, H. F., and Johnson, E., "Blunt-Body Wave Drag Reduction Using Focused Energy Addition," *AIAA Journal*, Vol. 37, No. 4, 1999, pp. 460–467.

[13]Luk'yanov, G. A., "Drag and Heat Exchange of an Object in a Supersonic Flow with a Planar Source of Energy in Front of the Object," *Technical Physics Letters*, Vol. 24, No. 12, 1998, pp. 980–982.

[14]Menart, J., Shang, J., Kimmel, R., and Hayes, J., "Total Drag and Lift Measurements in a Mach 5 Flow Affected by a Plasma Discharge and a Magnetic Field," AIAA Paper 2005-947, 2005.

[15]Kimmel, R., Hayes, J., Menart, J., and Shang, J., "Application of Plasma Discharge Arrays to High-Speed Flow Control," AIAA Paper 2005-946, 2005.

[16]Miles, R. B., Martinelli, L., Macheret, S. O., Girgis, I. G., Zaidi, S., Mansfield, D., Siclari, M., Smereczniak, P., Kashuba, R., and Vogel, P., "Suppression of Sonic Boom by Dynamic Off-Body Energy Addition and Shape Optimization," AIAA Paper 2002-0150, 2002.

[17]Macheret, S. O., Shneider, M. N., and Miles, R. B., "Potential Performance of Supersonic MHD Power Generators," AIAA Paper 2001-0795, 2001.

[18]Shneider, M. N., Macheret, S. O., and Miles, R. B., "Analysis of Magnetohydrodynamic Control of Scramjet Inlets," *AIAA Journal*, Vol. 42, No. 11, 2004, pp. 2302–2310.

[19]Myrabo, L. N., Raizer, Yu. P., and Shneider, M. N., "The Calculation and Similarity Theory of the Experiment Simulating the Air-Spike Effect in Hypersonic Aerodynamics," *High Temperature*, Vol. 36, No. 2, 1998, pp. 287–292.

[20]Bracken, R. M., Myrabo, L. N., Nagamatsu, H. T., Meloney, E. D., and Shneider, M. N., "Experimental Investigation of an Electric Arc Air-Spike in Mach 10 Flow with Preliminary Drag Measurements," AIAA Paper 2001-2734, 2001.

[21]Martinelli, L., Jameson, A., and Malfa, E., "Numerical Simulation of Three-Dimensional Vortex Flows over Delta Wing Configurations," *13th International Conference on Numerical Methods in Fluid Dynamics*, Vol. 414, Lecture Notes in Physics, edited by M. Napolitano and F. Solbetta, Springer-Verlag, 1992, pp. 534–538.

[22]Jameson, A., "Essential Elements of Computational Algorithms for Aerodynamic Analysis and Design," NASA CR-97-206268, Dec. 1997.

[23]Bychkov, V. L., Vasilev, M. N., and Zuev, A. P., "An Experimental and Theoretical Investigation of the Properties of Surface Electron-Beam Nitrogen Plasma," *High Temperature*, Vol. 32, No. 3, 1994, pp. 303–312.

[24]Sims, J. L., "Tables for Supersonic Flow Around Right Circular Cones at Small Angle of Attack," NASA SP-3007, 1964.

I. Boyd
Associate Editor